From ScOOH to Sc_2O_3: Phase Control, Luminescent Properties, and Applications

Baozhou Zhao, Xiaoji Xie, Shuilin Xu, Yue Pan, Bingxiao Yang, Shaohong Guo, Tian Wei, Haiquan Su, Haibo Wang, Xinqi Chen, Vinayak P. Dravid, Ling Huang, and Wei Huang**

The unique position of scandium (Sc) in the periodic table, i.e., the cross junction between the top of the rare earth column and the beginning of the transition metal row, has imparted unique chemical and physical properties to Sc and its compounds. For example, Sc lacks the 4f electrons and thus has different electronic configuration from other rare earth elements, and, unlike its counterparts, Sc does not follow the lanthanide contraction law.[1] In addition, the special physical and chemical properties have made Sc a popular additive to Al-, Mg-, and Ti-based alloys to improve their mechanical and electronic performances.[2,3]

In terms of Sc-based compounds, recent studies have discovered that cubic ScF_3 or its compound alloys, such as $Sc_{1-x}M_xF_3$ (M = Ga, Fe), have large negative or zero thermal expansion and even ferromagnetism if properly codoped, over a wide temperature range (10–1100 K), which is caused by the slightly twisted Sc-F or Sc/M–F–Sc/M linkage in the local structure of the crystals.[4]

B. Zhao, Dr. X. Xie, S. Xu, B. Yang, S. Guo, T. Wei, Prof. L. Huang, Prof. W. Huang
Key Laboratory of Flexible Electronics (KLOFE)
& Institute of Advanced Materials (IAM)
Jiangsu National Synergetic Innovation Center for Advanced Materials (SICAM)
Nanjing Tech University (NanjingTech)
Nanjing 211816, China
E-mail: iamlhuang@njtech.edu.cn; iamwhuang@njtech.edu.cn

Y. Pan, Prof. H. Su
School of Chemistry and Chemical Engineering
Inner Mongolia University
Hohhot 010022, China

Prof. H. Wang
Institute of Electric Light Source Materials
Nanjing Tech University (NanjingTech)
Nanjing 210015, China

Prof. X. Chen, Prof. V. P. Dravid
Department of Materials Science and Engineering
Northwestern University
Evanston, IL 60208, USA

Prof. X. Chen, Prof. V. P. Dravid
Northwestern University Atomic and Nanoscale Characterization Experimental (NUANCE) Center
Northwestern University
Evanston, IL 60208, USA

Prof. W. Huang
Key Laboratory for Organic Electronics and Information Displays
& Institute of Advanced Materials (IAM)
Jiangsu National Synergistic Innovation Center for Advanced Materials
Nanjing University of Posts and Telecommunications
Nanjing 210023, China

DOI: 10.1002/adma.201600960

On the other hand, due to the high refractive index (n_H = 2.0 at L = 300 nm), high bandgap (5.7 eV, corresponding to the UV cutoff at 215 nm), and high melting point (≈2480 °C), Sc_2O_3 can be potentially used for UV optical mirrors, shields, protective layers and polarizers,[5] high-reflection materials in light-emitting diodes (LEDs), high-power pulsed ultraviolet laser hosts, stabilizer for highly conducting ZrO_2-based solid electrolytes,[6] densifier in silicon nitride,[7] dopants in NO_x and CO_2 sensors,[8] and cathodes for high-resolution high-brightness cathode-ray tubes.[9] Unfortunately, the Sc_2O_3 described above are typically prepared via either isostatic compression followed by high-temperature (>1700 °C) sintering[10] or from direct crystal growth[11] at temperatures higher than 2000 °C, where costly facilities, cautious operation procedures, and time-consuming preparation are usually required. In this regard, easy-operation methods that allow the synthesis of Sc_2O_3 nanomaterials at low temperature and high quality are urgently desired.

Besides the mechanical, electronic, and catalytic properties, the unique luminescent properties of Sc-based nanomaterials have drawn significantly increased interest.[12–15] For example, we have reported that not only the chemical compositions and the corresponding crystal structures of Na_xScF_{3+x} are very sensitive to the synthesis experimental conditions, they also emit strong red upconversion luminescence when codoped with Yb^{3+}/Er^{3+}.[13a] This is different from those of the hexagonal phase nanomaterials of Yb^{3+}/Er^{3+} codoped Y- and lanthanide-based sodium fluorides, which usually generate strong green upconversion luminescence.[13,16] Subsequent luminescence studies have consistently confirmed that scandium fluorides are a series of unique crystal hosts for red upconversion emission when codoped with Yb^{3+}/Er^{3+}.[13–15]

Unfortunately, there are very few studies on the luminescent properties of Sc_2O_3,[15,17] and especially that Sc_2O_3 can work as a better host than Y_2O_3, for the cathodoluminescent light emission at certain concentrations.[17] Meanwhile, as a precursor for Sc_2O_3 synthesis, neither has there been any report on the luminescent properties of ScOOH.

In this study, we report the controlled synthesis of Sc_2O_3 nanomaterials via the precursor annealing of ScOOH, which can be easily synthesized in a hydrothermal method using sodium citrate as surfactant. More importantly, the morphology, size, crystal structure, and even the crystal phase transition of ScOOH can be easily achieved by simply varying the amount of surfactant molecules, which otherwise is not possible if surfactant molecules are not used.[18,19] The luminescence studies indicate that, similar to that of scandium fluorides, both Sc_2O_3:Ln and ScOOH:Ln (Ln = Yb/Er, Eu, Tb) can work as good

ADVANCED MATERIALS
www.advmat.de

Materials Views
www.MaterialsViews.com

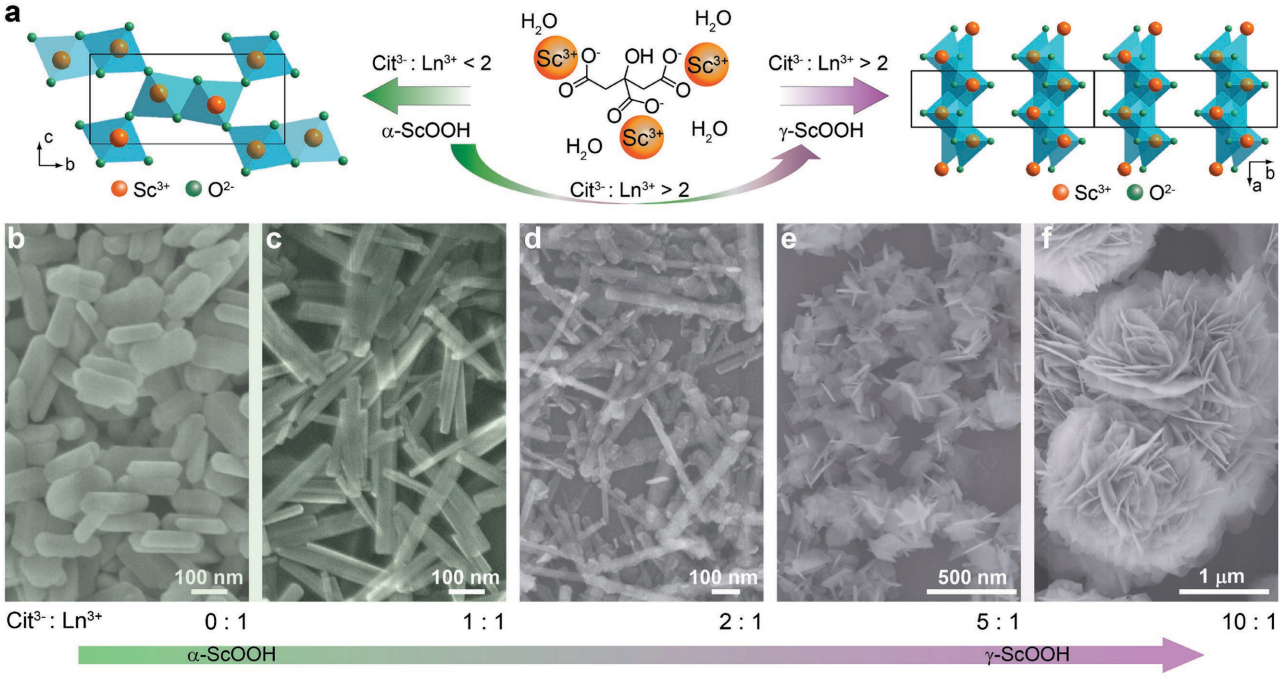

Figure 1. a) Schematic illustration of the relationship between the crystal structures of ScOOH nanomaterials and the Cit^{3-}:Ln^{3+} ratios (Cit^{3-}: trisodium citrate; Ln^{3+}: lanthanide chlorides). b-f) SEM images of the as-synthesized ScOOH nanomaterials with different Cit^{3-}:Ln^{3+} ratios: b) 0:1, c) 1:1, d) 2:1, e) 5:1, and f) 10:1.

crystal hosts for red upconversion emission when codoped with Yb^{3+}/Er^{3+}, which is consistent with our previous results.[13–15] Finally, high-temperature probing has been achieved based on the reverse temperature-dependent luminescent properties of ScOOH:Eu and ScOOH:Tb, while the LED performance has proved Sc_2O_3:Eu to be a better pure red luminescent material than Y_2O_3:Eu.

Typically, the formation of orthorhombic ScOOH could be elucidated by the olation-oxolation process under basic conditions, and depending on the types and amounts of bases used, the products could be α- or γ-phase ScOOH and the former one is thermodynamically more stable.[18,19] However, it is interesting to point out that our experimental results have suggested a different scenario where pure α-phase ScOOH nanorods with varying aspect ratios are obtained when the ratio of Cit^{3-}:Ln^{3+} is less than 2:1 (**Figure 1**b,c), but pure γ-phase ScOOH microflowers become the only product when Cit^{3-}:Ln^{3+} is larger than 2:1, and the size of the microflowers keeps increasing with the increment of the Cit^{3-}:Ln^{3+} ratio (Figure 1e,f). Zoomed-in Scanning electron microscopy (SEM) images indicate that the microflowers are assembled by many individual platelets with thickness at the nanoscale (Figure 1f). Logically, when the Cit^{3-}:Ln^{3+} ratio is set at 2, the mixture of α- and γ-phase ScOOH will be the product where the nanorods and small pieces of nanoplatelets can be clearly seen (Figure 1d).

More importantly, if α-ScOOH nanorods are further reacted with more Cit^{3-} (e.g., as long as the Cit^{3-}:Ln^{3+} ratio is higher than 2), α-ScOOH can be converted to γ-ScOOH. Further characterization suggests that this crystal structure conversion might be a process composed of the dissolution of α-ScOOH followed by the recrystallization of γ-ScOOH, as proved by the X-ray diffraction (XRD) and SEM data shown in Figure S1 (Supporting Information). This indicates that the phase transformation is due to the chemical binding of the Cit^{3-} ligands on the proper crystal facets,[20] which can be used for efficient control of both the morphology, size, crystal structure, and even the crystal phase transition of ScOOH nanomaterials.

Based on previous discussion, the relationship between the crystal structures of ScOOH nanomaterials and the Cit^{3-}:Ln^{3+} ratios is illustrated in Figure 1a. The evolution of the crystal structures of the final products corresponds very well with the gradual change of their respective XRD patterns (Figure S2, Supporting Information), and the Cit^{3-}:Ln^{3+} ratio of 2 is a turning point where mixed XRD patterns of both α- and γ-phase ScOOH are presented, while below and above this ratio, pure α- and γ-phase ScOOH can be obtained, respectively.

High-resolution transmission electron microscopy (HRTEM) images of the as-synthesized nanomaterials have confirmed the crystalline structures of both the nanorods and nanoplatelets in the microflowers (Figure S3, Supporting Information). Although the size of the resulting microflowers is large, they could be dispersed very well in water due to the good capping of Cit^{3-} ligands on the crystal facets. The Fourier transform infrared spectroscopy (FT-IR) spectra in Figure S4 (Supporting Information) further confirm the binding behavior of Cit^{3-} on the corresponding samples.

More intriguingly, the thermogravimetric analysis (TGA) and differential scanning calorimetry (DSC) analysis in **Figure 2** have shown that when Cit^{3-} is used as the capping agent, α-ScOOH:Tb began to decompose with about 13% weight loss at temperature below 440 °C, with an endothermic reaction peak at 437.3 °C on the DSC curve (Figure 2a), while

DOI: 10.1002/adma.201600960

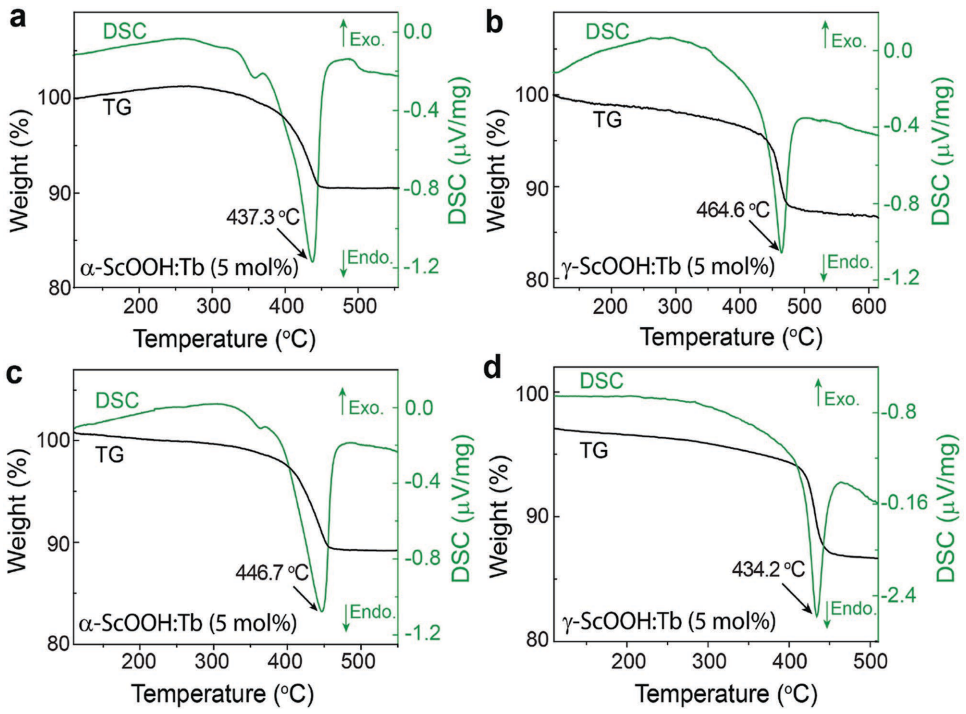

Figure 2. TGA-DSC curves of a) α-ScOOH:Tb and b) γ-ScOOH:Tb synthesized with Cit^{3-}, and c) α-ScOOH:Tb and d) γ-ScOOH:Tb synthesized without Cit^{3-}.

the endothermic process of Cit^{3-}-capped γ-ScOOH:Tb happens at 464.6 °C with about 13% weight loss. Here, the endothermic reaction peak of γ-ScOOH:Tb is about 27.3 °C higher than that of the α-ScOOH:Tb (Figure 2a,b), indicating that γ-ScOOH:Tb is the thermodynamically stable state while α-ScOOH:Tb becomes the metastable one when Cit^{3-} is used as a surfactant. This is opposite to previous report that α-ScOOH:Tb is thermodynamically more stable than γ-ScOOH:Tb when no surfactant is used,[19] as shown in Figure 2c,d, where the endothermic reaction peaks at 446.7 °C for α-ScOOH:Tb and at 434.2 °C for γ-ScOOH:Tb can be seen, respectively. The only difference is that in our experiment, Cit^{3-} is used as a surfactant, which further suggests that it is the Cit^{3-} binding on the crystal facet that causes the thermodynamical difference of α- and γ-ScOOH:Tb.

Furthermore, Figure 2a,c shows that the endothermic reaction peak of Cit^{3-}-capped α-ScOOH:Tb is 9.4 °C lower than that without Cit^{3-} binding, suggesting that Cit^{3-} binding makes α-ScOOH:Tb less stable. On the contrary, the endothermic reaction peaks of γ-ScOOH:Tb capped with Cit^{3-} is 30.4 °C higher than that of γ-ScOOH:Tb without Cit^{3-} (Figure 2b,d), suggesting that Cit^{3-} binding makes γ-ScOOH:Tb more stable.

Based on the above discussion, we can deduce that the binding force of Cit^{3-} on the surface of γ-ScOOH:Tb is stronger than that on α-ScOOH:Tb surface, which makes γ-ScOOH:Tb thermodynamically more stable than α-ScOOH:Tb.

On the other hand, the luminescence results in Figure S5a (Supporting Information) indicate that both α- and γ-ScOOH:Yb/Er (4/1 mol%) could emit red upconversion luminescence, which is consistent with previous reports on Sc-based nanomaterials.[12–16] The red luminescence generated from γ-ScOOH:Yb/Er is obviously much stronger than that of α-ScOOH:Yb/Er, which we think is mainly due to the larger size of the γ-ScOOH microflowers with less crystal defects compared to that of the α-ScOOH nanorods. The time-dependent reaction results indicated that 12 h hydrothermal synthesis could produce γ-phase ScOOH:Yb/Er (4/1 mol%) with the strongest upconversion luminescence (Figure S5b, Supporting Information).

In terms of the down-conversion luminescence, typical red and green emissions of γ-ScOOH:Eu and γ-ScOOH:Tb were observed under UV excitation (**Figure 3**a,b). A series of predesigned experimental results have shown that the optimized doping concentrations for Eu^{3+} and Tb^{3+} were at 6 and 5 mol% (Figure S6a,b, Supporting Information), respectively. The experimental results have also shown that the morphology of the microflowers changes with the increment of the doping concentration of both Eu^{3+} and Tb^{3+} ions (Figures S7 and S8, Supporting Information), i.e., the flower-shape gradually disappeared, which could be caused by the large ionic radii of the doped Eu^{3+} and Tb^{3+} ions. The doping of ions with large ionic radius may increase the electron charge density of crystal surface and thus slow the crystal growth, resulting in small and disassembled microflowers (Figure S7 and S8, Supporting Information).[21]

γ-ScOOH:Ln nanomaterials were then annealed in order to synthesize Sc_2O_3:Ln, and in the meanwhile, the –OH groups that usually quench the photoluminescence of lanthanide ions[22] were also removed, which resulted in the enhanced luminescence emission. Indeed, after 2 h annealing at 800 °C, orthorhombic γ-ScOOH:Yb/Er converted to cubic Sc_2O_3:Yb/Er with the microflower shape maintained, which can be confirmed by both the XRD results (Figure S9a, Supporting Information)

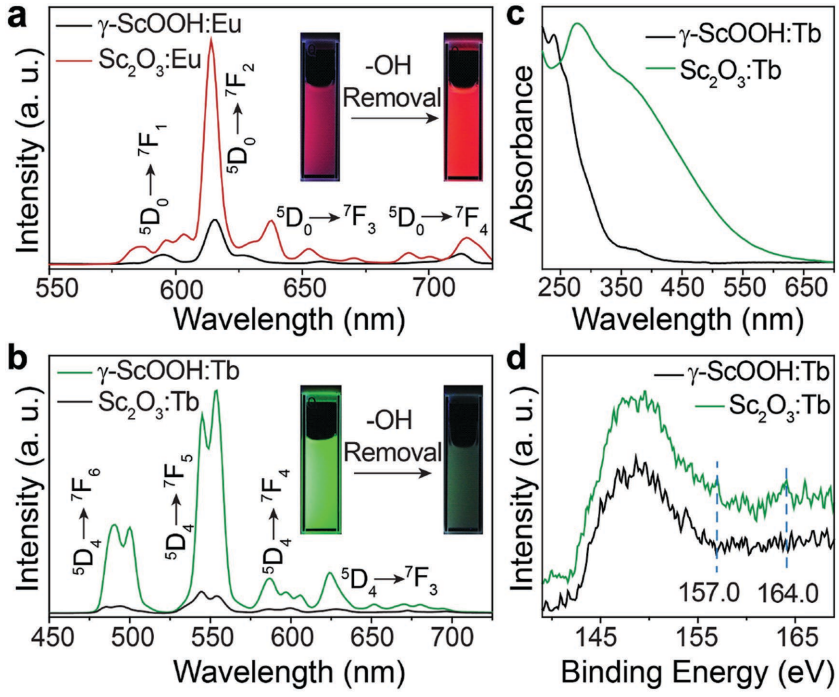

Figure 3. Room-temperature luminescence emission spectra of a) γ-ScOOH and Sc_2O_3 microflowers doped with Eu^{3+} (6 mol%) under 250 nm UV excitation and b) γ-ScOOH and Sc_2O_3 doped with Tb^{3+} (5 mol%) under 265 nm UV excitation. The insets in (a) and (b) are the corresponding digital luminescent photos of aqueous solutions containing ≈1.0 mg mL^{-1} nanomaterials. c) Normalized solid state UV-vis absorption spectra of the samples shown in (b). d) XPS analysis of γ-ScOOH:Tb (20 mol%) microflowers and corresponding Sc_2O_3:Tb obtained after thermal annealing.

and the corresponding SEM images before and after annealing (Figure S9b,c, Supporting Information). More importantly, the enhancement of the upconversion luminescence was observed after thermal annealing (Figure S10, Supporting Information). It is worthy to emphasize that α-ScOOH:Yb/Er also converted to cubic Sc_2O_3:Yb/Er after annealing, with the same nanorod morphology (Figure S11a-c, Supporting Information) and the luminescence emission dramatically increased (Figure S11d, Supporting Information).

Similarly, after the same annealing, γ-ScOOH:Eu and γ-ScOOH:Tb changed to Sc_2O_3:Eu and Sc_2O_3:Tb (Figure S12, Supporting Information), respectively, and as expected, a dramatic increase in Eu^{3+} emission was obtained (Figure 3a; Figure S13a, Supporting Information). In addition, a notable increase in luminescence lifetime of Eu^{3+} emission at 615 nm was observed, which indicates suppressed nonradiative energy transfer (Figure S14a, Supporting Information). However, a surprisingly large emission intensity decrease of Tb^{3+} was seen after the same annealing process in the case of γ-ScOOH:Tb (5 mol%), as shown in Figure 3b and Figure S13b (Supporting Information). Further luminescence lifetime study of Tb^{3+} emission at 554 nm reveals increased nonradiative energy transfer after thermal annealing (Figure S14b, Supporting Information). The successful doping of the lanthanide ions into each sample can be proved by the inductively coupled plasma atomic emission spectroscopy (ICP-AES) data (Table S1, Supporting Information).

To gain more insight into the luminescence emission drop, the UV absorption spectra of the samples before (γ-ScOOH:Tb) and after (Sc_2O_3:Tb) annealing were recorded in Figure 3c where a plausible absorption peak at ≈350 nm can be clearly seen in Sc_2O_3:Tb, while no such absorption peak can observed in either ScOOH:Tb (Figure 3c) or Eu^{3+}-doped nanomaterials (Figure S15, Supporting Information). This wide absorption can be assigned to the typical charge transfer band of Tb^{4+}, which obviously is originated from Tb^{3+} in Sc_2O_3:Tb, indicating that Tb^{3+} was partially oxidized to Tb^{4+} during the thermal annealing process.[23] In order to exclude the possibility of oxidation by the oxygen from the air, the annealing experiment was carried out under nitrogen protection and the Tb^{4+} absorption still exists though became obviously weakened (Figure S16a, Supporting Information). This suggests that the oxidation of Tb^{3+} to Tb^{4+} happens from inside of the nanocrystal itself, i.e., the intrinsic oxygen defects in the nanocrystals, which cannot be avoided even under the reductive environment of the mixture of H_2 and Ar (Figure S16a, Supporting Information). Sequentially, the luminescence intensity of the samples annealed under different environment is proportionally related to the extent of the Tb^{3+} oxidation (Figure S16b, Supporting Information). This again, clearly proves the high tendency of Tb^{3+} oxidation, which should be responsible for the decreased luminescence intensity of γ-ScOOH:Tb after annealing.

Parallelly, the appearance of two new peaks at 157.0 and 164.0 eV (Figure 3d) from the X-ray photoelectron spectroscopy (XPS) studies on annealed γ-ScOOH:Tb, i.e., Sc_2O_3:Tb, is regarded as the direct evidence of the chemical state change of Tb^{3+} ions after thermal annealing, and this data corresponds very well with the XPS data of standard Tb^{3+} in Tb_2O_3 (Figure S17a, Supporting Information) and Tb^{4+} in Tb_4O_7 (Figure S17b, Supporting Information) powders, respectively. The typical four XPS peaks of Tb^{3+} at 145.23, 147.93, 150.83, and 154.63 eV in Tb_2O_3 can be found accordingly in the XPS spectrum of Tb_4O_7 at 146.03, 148.38, 151.03, and 153.83 eV, respectively. However, the peaks at 157.28 and 164.48 eV in Tb_4O_7,[24] obviously originated from Tb^{4+}, cannot be seen in Tb_2O_3, but they correspond very well with the XPS peaks at 157.0 and 164.0 eV in the annealed ScOOH:Tb, i.e., Sc_2O_3:Tb (Figure 3d). This straightforwardly suggests that the oxidation reaction from Tb^{3+} to Tb^{4+} has happened during the annealing process of ScOOH:Tb, which has made us believe that the partial oxidation of Tb^{3+} and the corresponding microenvironmental changes after thermal annealing is responsible for the dramatically weakened luminescence emission of Tb^{3+}.

From the application point of view, the reverse dependence of the luminescence intensity of γ-ScOOH:Eu and γ-ScOOH:Tb on temperature, has made their combinatorial components

Adv. Mater. 2016,
DOI: 10.1002/adma.201600960

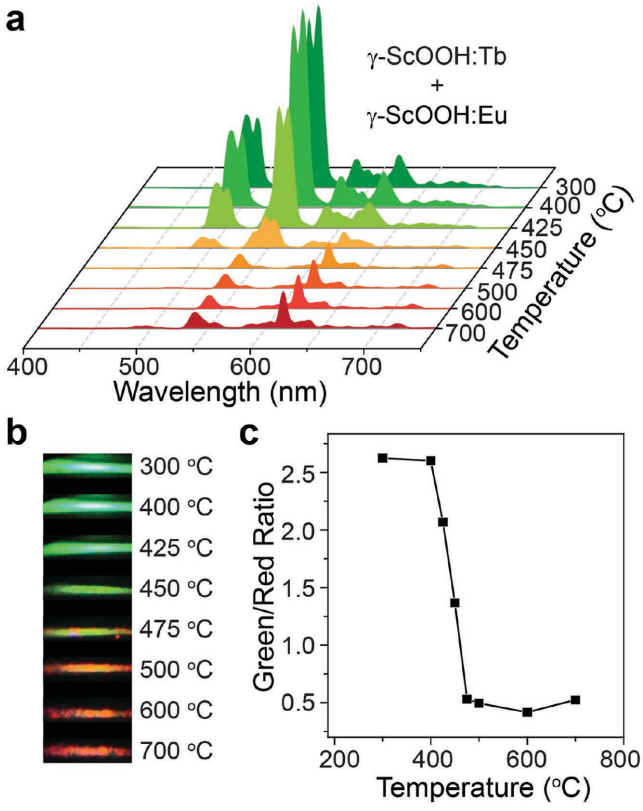

Figure 4. a) Room temperature luminescence emission spectra of the γ-ScOOH:Tb (5 mol%) and γ-ScOOH:Eu (6 mol%) mixture after incubated at different temperatures under 265 nm excitation. b) The corresponding luminescent digital photos of samples at different temperatures and c) the temperature-dependence of the green-to-red ratios, respectively.

ideal candidates for colorimetric high-temperature probing. To demonstrate this, the test slides were first prepared by simply mixing γ-ScOOH:Tb and γ-ScOOH:Eu microflowers and then incubated at various temperatures. As can be seen from the luminescence spectra of the mixture of γ-ScOOH:Tb and γ-ScOOH:Eu in **Figure 4**a, the green emission of Tb^{3+} at 550 nm started to decrease when the temperature is higher than 425 °C whereas the red emission of Eu^{3+} at 610 nm started dominating the whole emission as the samples are heated above 500 °C.[25] Under 265 nm UV light excitation, a continuous emission color change of the test slides at different temperatures can be easily interpreted to the corresponding temperature range (Figure 4b). More interestingly, the green/red ratio changed sharply with the temperature variation, suggesting the capability of temperature probing at high sensitivity. In the meanwhile, the plot of the green/red ratio with temperature in Figure 4c is almost identical to the TGA plot of γ-ScOOH microflowers (Figure 2b). This is reasonable because γ-ScOOH started to dissociate to Sc_2O_3 at elevated temperatures in the TGA plot whereas the γ-ScOOH:Ln in Figure 4b is actually dissociating during the temperature probing process, i.e., both of the plots reflect the actual chemical reactions happening during this heating process.

Considering the luminescent properties of ScOOH:Eu and Sc_2O_3:Eu, a series of proof-of-concept LEDs were fabricated.

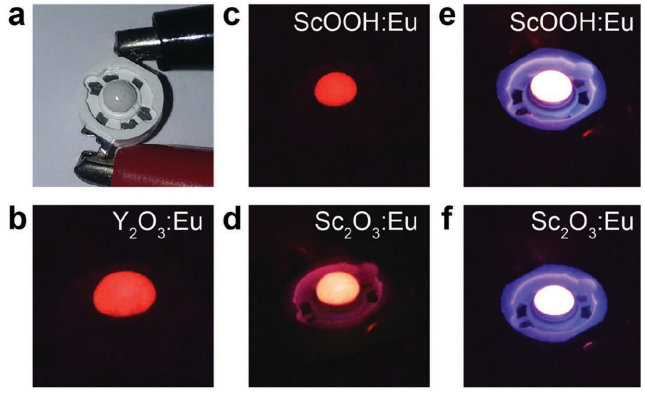

Figure 5. Digital photos of red and white light-emitting diodes fabricated using ScOOH:Eu (6 mol%), Sc_2O_3:Eu (6 mol%), Y_2O_3:Eu (6 mol%) nanomaterials, respectively. a) The digital photo of LED with voltage off, and b-f) are photos taken with voltage on.

As shown in **Figure 5**, LED fabricated using ScOOH:Eu gives very pure red emission, and the Sc_2O_3:Eu-based LED generates even brighter red light emission. Their corresponding luminescence spectra indicate that both ScOOH:Eu and Sc_2O_3:Eu can emit very pure red light at 611 nm with full width at half maximum (FWHM) of ≈6.9 nm (Figure S18b,c, Supporting Information). This is much narrower than that of the commercially used nitride-based luminescent material with the FWHM to be ≈83.3 nm, which actually covers the green, yellow, and red emission (Figure S18a, Supporting Information).

What is more, the Commission Internationale de l'Eclairage (CIE) coordinates for ScOOH:Eu and Sc_2O_3:Eu (Figure S18e, Supporting Information) are determined at (0.603, 0.396) and (0.613, 0.386), indicating that they can generate pure red emission and can be used as pure red luminescent materials for white-light LED purpose. Indeed, by mixing with the yellow luminescent material (YAG:Ce), the white-light LEDs using both ScOOH:Eu and Sc_2O_3:Eu were fabricated respectively, and both of them give very strong white light (Figure 5e,f). The stability test indicates that the LEDs can work very steadily after continuous lighting for over 2160 h. It is worth to notify that as luminescent material for lighting purpose, Sc_2O_3:Eu gives brighter emission than that of Y_2O_3:Eu (Figure 5b,d), though Y_2O_3:Eu has similar FWHM of ≈6.9 nm (Figure S18d, Supporting Information) and CIE coordinates at (0.594, 0.406). As a comparison, the coordinates of commercially used nitride at (0.622, 0.378) further indicates that Sc_2O_3:Eu can be a good candidate as red phosphor for lighting. Further luminous efficacy measurement of the fabricated red LEDs gives 38.31 and 32.26 lm W^{-1} for Sc_2O_3:Eu- and Y_2O_3:Eu-based LEDs, respectively, suggesting that Sc_2O_3:Eu can be a better luminescent material than Y_2O_3:Eu, which is also consistent with previous report.[17]

In conclusion, we have achieved controlled synthesis of Sc_2O_3 via the annealing of ScOOH. The surfactant molecules used can help to induce the phase transformation from α- to γ-ScOOH, which is not possible if Cit^{3-} is not used. The XPS results of γ-ScOOH:Tb and Sc_2O_3:Tb have disclosed that the cause of the weakened luminescence emission of Tb^{3+} was due to the partial oxidation of Tb^{3+} from the intrinsic oxygen defects within the nanocrystal. Finally, the applications of γ-ScOOH:Ln

and Sc_2O_3:Ln for both high-temperature probing and LED lighting were proved where Sc_2O_3:Eu shows better performance than Y_2O_3:Eu. We believe the results discovered on ScOOH:Ln and Sc_2O_3:Ln will further complement the fundamental studies on Sc-based compounds and will also greatly widen the potential applications of Sc-based nanomaterials.

Experimental Section

Experimental details can be found in the Supporting Information.

Supporting Information

Supporting Information is available from the Wiley Online Library or from the author.

Acknowledgements

B.Z. and X.X. contributed equally to this work. This work was supported by the National Natural Science Foundation of China (Grant Nos. 21371095, 61136003, and 21401103) and the Natural Science Foundation of Jiangsu Province (Grant Nos. BL2014075, BM2012010, and BK20131404). This project was also supported by the Specially Appointed Professors of the Jiangsu Province, the Synergetic Innovation Center for Organic Electronics and Displays, and the National Science Foundation's MRSEC program (Grant No. DMR-1121262), and made use of its Shared Facilities at the Materials Research Center of Northwestern University.

Received: February 18, 2016
Revised: March 23, 2016
Published online:

[1] a) L. Fornasiero, E. Mix, V. Peters, K. Petermann, G. Huber, *Cryst. Res. Technol.* **1999**, *34*, 255; b) N. T. McDevitt, A. D. Davidson, *J. Opt. Soc. Am.* **1966**, *56*, 636.

[2] a) F. von Buch, J. Lietzau, B. L. Mordike, A. Pisch, R. S. Fetzer, *Mater. Sci. Eng., A* **1999**, *263*, 1; b) A. Sehirlioglu, A. Sayir, F. Dynys, *J. Am. Ceram. Soc.* **2008**, *91*, 2910; c) E. A. Marquis, D. N. Seidman, *Acta Mater.* **2005**, *53*, 4259.

[3] a) Y. Deng, B. Peng, G. Xu, Q. Pan, Z. Yin, R. Ye, Y. Wang, L. Lu, *Mater. Sci. Eng., A* **2015**, *639*, 500; b) S. Ge, M. Celikin, M. Isac, R. I. L. Guthrie, *Metall. Mater. Trans. B* **2015**, *46B*, 1035.

[4] a) J. P. Attfield, *Nature* **2011**, *480*, 465; b) L. Hu, J. Chen, L. Fan, Y. Ren, Y. Rong, Zhao Pan, J. Deng, R. Yu, X. Xing, *J. Am. Chem. Soc.* **2014**, *136*, 13566; c) C. R. Morelock, L. C. Gallington, A. P. Wilkinson, *Chem. Mater.* **2014**, *26*, 1936; d) C. W. Li, X. Tang, J. A. Muñoz, J. B. Keith, S. J. Tracy, D. L. Abernathy, B. Fultz, *Phys. Rev. Lett.* **2011**, *107*, 195504; e) B. K. Greve, K. L. Martin, P. L. Lee, P. J. Chupas, K. W. Chapman, A. P. Wilkinson, *J. Am. Chem. Soc.* **2010**, *132*, 15496.

[5] a) D. Grosso, P. A. Sermon, *J. Mater. Chem.* **2000**, *10*, 359; b) B. Keszei, J. Paitz, J. Vandlik, A. Süveges, *J. Cryst. Growth* **2001**, *226*, 95.

[6] S. P. S. Badwal, F. T. Ciacchi, D. Milosevic, *Solid State Ionics* **2000**, *136–137*, 91.

[7] D. S. Cheong, W. A. Sander, *J. Am. Ceram. Soc.* **1992**, *75*, 3331.

[8] a) N. Imanaka, S. Banno, G. Adachi, *Chem. Lett.* **1994**, *2*, 319; b) S. Tamura, N. Imanaka, M. Kamikawa, G. Adachi, *Sens. Actuators, B* **2001**, *73*, 205; c) X. Zhang, A. B. Walters, M. A. Vannice, *Appl. Catal., B* **1994**, *4*, 237; d) X. Zhang, A. B. Walters, M. A. Vannice, *J. Catal.* **1995**, *155*, 290; e) K. Otsuka, Q. Zhang, I. Yamanaka, H. Tono, M. Hatano, H. Kinoshita, *Bull. Chem. Soc. Jpn.* **1996**, *69*, 3367.

[9] E. Uda, O. Nakamura, S. Matsumoto, T. Higuchi, *Appl. Surf. Sci.* **1999**, *146*, 31.

[10] a) A. Lupei, V. Lupei, C. Gheorghe, A. Ikesue, *J. Lumin.* **2008**, *128*, 918; b) A. Lupei, V. Lupei, C. Gheorghe, A. Ikesue, E. Osiac, *Opt. Mater.* **2009**, *31*, 744.

[11] a) S. Kück, L. Fornasiero, E. Mix, G. Huber, *J. Lumin.* **2000**, *87–89*, 1122; b) R. Simura, A. Jouini, M. J. Hun, A. Brenier, A. Yoshikawa, G. Boulon, T. Fukuda, *Opt. Mater.* **2007**, *30*, 18.

[12] a) H. Chang, Y. Zhu, J. Xie, H. Li, B. Liu, S. Xu, X. Xie, L. Huang, W. Huang, *J. Mater. Chem. C* **2015**, *48*, 12385; b) W. Pei, B. Chen, L. Wang, J. Wu, X. Teng, R. Lau, L. Huang, W. Huang, *Nanoscale* **2015**, *7*, 4048; c) I. Vedel, F. Clerc, C. Chateau, J.M. Léger, *Mater. Res. Bull.* **1985**, *20*, 1213; d) S. Hao, L. Sun, G. Chen, H. Qiu, C. Xu, T. N. Soitah, Y. Sun, C. Yang, *J. Alloys Compd.* **2012**, *522*, 74; e) M. Pang, J. Feng, S. Song, Z. Wang, H. Zhang, *Cryst. Eng. Commun.* **2013**, *15*, 6901; f) X. He, B. Yan, *Cryst. Growth Des.* **2014**, *14*, 3257; g) H. Chang, J. Xie, B. Zhao, B. Liu, S. Xu, N. Ren, X. Xie, L. Huang, W. Huang, *Nanomaterials* **2015**, *5*, 1; h) Y. Ding, X. Zhang, H. Zhua, J. Zhu, *J. Mater. Chem. C* **2014**, *2*, 946; i) F. Kang, X. Yang, M. Peng, L. Wondraczek, Z. Ma, Q. Zhang, J. Qiu, *J. Phys. Chem. C* **2014**, *118*, 7515; j) L. Han, Y. Wang, L. Guo, L. Zhao, Y. Tao, *Nanoscale* **2014**, *6*, 5907.

[13] a) X. Teng, Y. Zhu, W. Wei, S. Wang, J. Huang, R. Naccache, W. Hu, A. I. Y. Tok, Y. Han, Q. Zhang, Q. Fan, W. Huang, J. A. Capobianco, L. Huang, *J. Am. Chem. Soc.* **2012**, *134*, 8340; b) W. Pei, L. Wang, J. Wu, B. Chen, W. Wei, R. Lau, L. Huang, W. Huang, *Cryst. Growth Des.* **2015**, *15*, 2988.

[14] a) Y. Ding, X. Teng, H. Zhu, L. Wang, W. Pei, J. J. Zhu, L. Huang, W. Huang, *Nanoscale* **2013**, *5*, 11928; b) Y. Ai, D. Tu, W. Zheng, Y. Liu, J. Kong, P. Hu, Z. Chen, M. Huang, X. Chen, *Nanoscale* **2013**, *5*, 6430; c) M. Pang, X. Zhai, J. Feng, S. Song, R. Deng, Z. Wang, S. Yao, X. Ge, H. Zhang, *Dalton Trans.* **2014**, *43*, 10202.

[15] a) H. Kuehn, M. Fechner, A. Kahn, H. Scheife, G. Huber, *Opt. Mater.* **2009**, *31*, 1636; b) C. Gheorghe, A. Lupei, V. Lupei, L. Gheorghe, A. Ikesue, *J Appl. Phys.* **2009**, *105*, 123110; c) A. Fukabori, V. Chani, K. Kamada, F. Moretti, A. Yoshikawa, *Cryst. Growth Des.* **2011**, *11*, 2404; d) D. Li, W. Qin, S. Liu, W. Pei, Z. Wang, P. Zhang, L. Wang, L. Huang, *J. Alloys Compd.* **2015**, *653*, 304.

[16] a) K. Kraemer, D. Biner, G. Frei, H. U. Guedel, M. P. Hehlen, S. R. Luethi, *Chem. Mater.* **2004**, *16*, 1244; b) X. Liu, R. Deng, Y. Zhang, Y. Wang, H. Chang, L. Huang, X. Liu, *Chem. Soc. Rev.* **2015**, *44*, 1479; c) W. Zheng, S. Zhou, Z. Chen, P. Hu, Y. Liu, D. Tu, H. Zhu, R. Li, M. Huang, X. Chen, *Angew. Chem. Int. Ed.* **2013**, *52*, 6671; d) V. Mahalingam, F. Vetrone, R. Naccache, A. Speghini, J. A. Capobianco, *Adv. Mater.* **2009**, *21*, 4025; e) S. Sivakumar, F. C. J. M. van Veggel, M. Raudsepp, *J. Am. Chem. Soc.* **2005**, *127*, 12464; f) H. S. Qian, Y. Zhang, *Langmuir* **2008**, *24*, 12123; g) N. Niu, P. Yang, F. He, X. Zhang, S. Gai, C. Li, J. Lin, *Nanoscale* **2012**, *22*, 10889; h) J. Zhao, D. Jin, E. P. Schartner, Y. Lu, Y. Liu, A. V. Zvyagin, L. Zhang, J. M. Dawes, P. Xi, J. A. Piper, E. M. Goldys, T. M. Monro, *Nat. Nanotechnol.* **2013**, *8*, 729.

[17] D. Gozzi, A. Latini, D. Carta, A. Corrias, A. Falqui, G. Mountjoy, L. Lazzarini, G. Salviati, S. G. Fiddy, *Chem. Mater.* **2008**, *20*, 5666.

[18] a) V. Ripert, L. G. Hubert-Pfalzgarf Pfalzgraf, R. Papiernik, P. Belleville, H. Floch, *J. Mater. Chem.* **2001**, *11*, 1880; b) J. Li,

T. Ikegami, T. Mori, Y. Yajima, *J. Mater. Res.* **2003**, *18*, 1149; c) W. O. Milligan, J. L. McAtee. *J. Phys. Chem.* **1956**, *60*, 273; d) A. N. Christensen, S. J. Jensen, *Acta Chem. Scand.* **1967**, *21*, 121.

[19] Y.-W. Zhang, J. Liu, R. Si, Z. Yan, C.-H. Yan, *J. Phys. Chem. B* **2005**, *109*, 18324.

[20] a) L. Qian, J. Zhu; Z. Chen; Y. Gui, Q. Gong, Y. Yuan, J. Zai, X. Qian, *Chem. Eur. J.* **2009**, *15*, 1233; b) C. Li, Z. Hou, C. Zhang, P. Yang, G. Li, Z. Xu, Y. Fan, J. Lin, *Chem. Mater.* **2009**, *21*, 4598.

[21] F. Wang, Y. Han, C. S. Lim, Y. Lu, J. Wang, J. Xu, H. Chen, C. Zhang, M. Hong, X. Liu, *Nature* **2010**, *463*, 1061.

[22] a) W. Di, X. Wang, B. Chen, S. Lu, X. Zhao, *J. Phys. Chem. B* **2005**, *109*, 13154; b) H. Hayashia, N. Sugimoto, S. Tanabe, S. Ohara, *J. Appl. Phys.* **2006**, *99*, 093105.

[23] H. Hosono, T. Kinoshita, H. Kawazoe, M. Yamazaki, Y. Yamamoto, N. Sawanobori, *J. Phys.: Condens. Matter.* **1998**, *10*, 9541.

[24] S. V. Belaya, V. V. Bakovets, A. I. Boronin, S. V. Koshcheev, M. N. Lobzareva, I. V. Korolkov, P. A. Stabnikov, *Inorg. Mater.* **2014**, *50*, 379.

[25] a) T. Selvalakshmi, S. Sellaiyan, A. Uedono, A. C. Bose, *Mater. Chem. Phys.* **2015**, *166*, 73; b) K. G. Sharma, N. S. Singh, Y. R. Devi, N. R. Singh, S. D. Singh, *J. Alloys Compd.* **2013**, *556*, 94.